International Journal of Hydrogen Energy 59 (2024) 1507–1517

Contents lists available at ScienceDirect

International Journal of Hydrogen Energy

journal homepage: www.elsevier.com/locate/he

Thermodynamic and exergoeconomic analyses of a novel biomass-fired combined cycle with solar energy and hydrogen and freshwater production in sports arenas

Shayan Sharafi Laleh [a], Ali Safarpour [b], Arash Shahbazi Shahrak [c], Seyed Hamed Fatemi Alavi [a], Saeed Soltani [d,*]

[a] Faculty of Mechanical Engineering, University of Tabriz, 16471, Tabriz, Iran
[b] Faculty of Physical Education and Sport Sciences, Department of Sport Management, Tehran University, 35840, Tehran, Iran
[c] Engineering Islamic Azad University Ilkhchi Branch, 14418, Ilkhchi, Iran
[d] Faculty of Engineering and Natural Sciences, Antalya Bilim University, 07190, Antalya, Turkey

ARTICLE INFO

Keywords:
Renewable energy
Sports facilities
Hydrogen production
Reverse osmosis
Water purification
Solar energy

ABSTRACT

In this article to tackle the main concerns of today's world as fossil fuel shortage, environmental impacts of fossil fuels like global warming and atmosphere pollution as well as water scarcity, a novel power plant is designed. In this regard, the proposed plant comprises of biomass gasification unit, photovoltaic thermal collectors, a proton exchange membrane hydrogen production unit, as well as a reverse osmosis water purification plant. The plant is named as (biomass-fired combined cycle with photovoltaic, thermal collectors, hydrogen production, and reverse osmosis) BCPVHR and to assess its performance, energy, exergy, exergoeconomic, and environmental analyses are performed. The varying parameters are compressor pressure ratio and gas turbine inlet temperature. These two parameters' impact on energy efficiency, exergy efficiency, net generated power, fresh water production, total unit product cost as well and environmental index are assessed. The results are useful for adjusting the compressor pressure ratio and gas turbine inlet temperature. Please note that this plant is designed to be used completely or partially in sports facilities and can be a valuable endeavor for managing sports facilities to use renewable energy in their construction. Meanwhile, based on the priories of products different values of parameters can be used. Increasing the compressor pressure ratio raises the total unit product cost and the environmental index until 11.5 decreases and later increases. Increasing the gas turbine inlet temperature decreases the both total unit product cost and environmental index which reach 65 $/GJ and 65 kg/kWh, respectively.

1. Introduction

In contemporary society, the imperative to transition towards sustainable and renewable energy sources has become increasingly pronounced, driven by the urgent need to address environmental concerns and the detrimental impact of fossil fuels on both human health and the planet [1]. Renewable energy, characterized by its low environmental impact and infinite availability, stands as a beacon of hope in mitigating climate change and fostering a cleaner, healthier future. It is crucial to be completely aligned with the development of sustainable energy which empowers vulnerable people, especially in remote areas, offering them free energy as well as sustainable-based commodities such as clean water [2,3]. Renewable energy sources, including solar, wind, hydro, and geothermal power, have emerged as pivotal alternatives to traditional fossil fuels [4]. The inherent sustainability of renewable sources stems from their capacity for natural replenishment, offering a perpetual and environmentally friendly energy solution [4,5]. These sources not only reduce greenhouse gas emissions but also diminish dependence on finite fossil fuel reserves, thereby contributing to a more sustainable and resilient energy landscape [2]. Further exploration of advanced technologies, such as energy storage systems and smart grids, ensures the integration of renewable energy into existing infrastructures [6–8]. Recent developments in materials science, as highlighted by Wang et al., present promising avenues for enhancing the efficiency and viability of solar energy technologies [6,9].

In recent years, the sports industry has embraced the ethos of sustainability, with a growing number of organizations and events adopting

* Corresponding author.
E-mail addresses: soltani929@gmail.com, saeed.soltani@antalya.edu.tr (S. Soltani).

https://doi.org/10.1016/j.ijhydene.2024.02.146
Received 13 December 2023; Received in revised form 5 February 2024; Accepted 10 February 2024
Available online 16 February 2024

Nomenclature

b	Width of PVT collector (m)
c	Cost per unit exergy ($/GJ)
$\dot{C}$	Cost rate ($/h)
D	Membrane thickness (μm)
E	Reversible potential (V)
$E_{act,a}$	The activation energy of anode (kJ/mol)
$\dot{E}$	Exergy rate (kW)
f	Exergoeconomic factor
F	Faraday constant (C/mol)
h_{p1G}	Penalty factor due to the presence of solar cell material, glass, and EVA for glass-to-glass PVT system
h_{p2G}	Penalty factor due to the presence of an interface between glass and working fluid through the absorber plate for glass-to-glass PVT system
$\dot{I}$	Solar radiation intensity (kW/m^2)
J_a^{ref}	Pre-exponential factor of anode (A/m^2)
J_c^{ref}	The pre-exponential factor of the cathode (A/m^2)
L	Length of PVT collector (m)
LOCP	Levelized overall cost of products
$\dot{m}$	Mass flow rate (kg/s)
N	Number of cells in PEM electrolyzer
P	Pressure (kPa)
r_p	Pressure ratio
$\dot{Q}$	Heat rate (kW)
T	Temperature (K)
U_L	Overall heat transfer coefficient from solar cell to ambient through top and back surface of insulation (W/m^2 K)
$\dot{W}$	Power (kW)
$\dot{Z}$	Investment cost rate ($/h)
Z_k	Investment cost of component k ($)

Abbreviations

AC	Air compressor
BCPVHR	Plant comprises of biomass gasification unit, photovoltaic thermal collectors, proton exchange membrane hydrogen production unit, as well as reverse osmosis water purification plant
CC	Combustion chamber
CRF	Capital recovery factor
GT	Gas turbine
GTIT	Gas turbine inlet temperature
LCOP	Levelized overall cost of products
ORC	organic Rankine cycle
PEM	Proton Exchange Membrane
PVT	Thermal photovoltaic
RO	Reverse osmosis

Greek letters

α_b	Absorptivity of the black surface
α_c	Absorptivity of solar cell
β_c	Packing factor of solar cell
η_{is}	Isentropic efficiency
σ (x)	Local ionic PEM conductivity (S/m)
σ_{PEM}	Proton conductivity in PEM (S/m)
τ_g	Transmissivity of glass
λ_a	Water content at anode-membrane interface
λ_c	Water content at the cathode-membrane interface

Subscripts

AC	Air compressor
Cond	Condenser
g	Gasifier
GT	Gas turbine
HTR	High-temperature recuperator
LTR	Low-temperature recuperator
Pu	Pump
Reg	Regenerator
REC	Recuperator
ST	Steam turbine

renewable energy solutions [10]. Stadiums and facilities powered by solar panels, wind turbines, and other green technologies exemplify a commitment to reducing the environmental footprint of sporting events [11]. This intersection between sports and renewable energy not only exemplifies a commitment to environmental stewardship but also serves as a powerful platform to raise awareness and inspire collective action [12]. Studies shed light on the positive impact of sustainable practices in sports on fan engagement and corporate partnerships [13]. The incorporation of renewable energy technologies in sports facilities contributes to creating more sustainable and eco-friendly sporting environments [10–16]. In this context, examining the integration of renewable energy in the sports sector becomes not only an environmental imperative, but also a catalyst for promoting sustainable practices and fostering a global commitment to a cleaner, healthier future [15,17–19].

Biomass gasification stands as a prominent and versatile technology in the realm of sustainable energy, offering a pathway to harness renewable energy from organic sources [3,20,21]. The integration of biomass gasification into energy systems contributes to the diversification of renewable energy sources [22,23], aiding in the reduction of greenhouse gas emissions and mitigating climate change [24]. Recent advancements in gasification technologies, such as fluidized bed reactors and downdraft gasifiers, have improved efficiency and expanded the range of biomass feedstock applicable for gasification [23,25,26]. Additionally, the coupling of biomass gasification with other clean energy technologies, like combined heat and power systems and advanced gas cleaning methods, further enhances its viability in sustainable energy systems [24]. As the global focus intensifies on achieving a transition to low-carbon energy, biomass gasification emerges as a pivotal player in shaping a resilient and eco-friendly energy landscape [25].

Proton Exchange Membrane (PEM) electrolyzers have gained prominence as efficient and environmentally friendly devices for hydrogen production through water electrolysis [27,28]. This technology holds promise for scalable and clean hydrogen generation, playing a vital role in the advancement of the hydrogen economy [29]. Recent research has focused on enhancing PEM electrolyzer performance through advancements in catalyst materials, membrane technologies, and system integration. Studies delve into novel catalyst designs, while advancements in membrane technology [30]. Additionally, studies highlight the integration of PEM electrolyzers with renewable energy sources, emphasizing the potential for sustainable hydrogen production [27,28,31].

Thermal photovoltaic (PVT) systems represent an innovative approach to solar energy harvesting, combining traditional photovoltaic technology with thermal energy capture to enhance overall efficiency [32,33]. These systems utilize the absorbed sunlight not only for electricity generation but also for the extraction of thermal energy, offering a dual-purpose solution [34]. The integration of thermal components aids in cooling the photovoltaic cells, improving their performance and longevity [35]. Recent research in this field has explored advanced materials and designs to optimize the synergistic relationship between photovoltaics and thermal elements [34]. Studies investigate novel

materials for enhanced thermal management, while some studies delve into innovative system designs and configurations [36].

Reverse osmosis (RO) stands as a pivotal technology in the realm of desalination and water purification, offering an energy-efficient and widely adopted solution for producing fresh water from saline or contaminated water sources [37–39] This process relies on a semi-permeable membrane to selectively allow water molecules to pass through while blocking impurities and salts [38]. Recent advancements in reverse osmosis technology have focused on improving membrane materials, system efficiency, and sustainability [40]. Studies discuss the development of high-performance membranes with enhanced rejection capabilities [37]. Additionally, some studies explore innovative approaches to improve the energy efficiency of reverse osmosis systems. The integration of advanced materials, such as graphene oxide, has enhanced the durability and performance of RO membranes, showcasing the continuous evolution of reverse osmosis as a crucial technology for sustainable water management [41].

Based on research data on the realm of renewable energies and freshwater production it is evident that still there is much room for a scientist to pursue their studies. To this end, we proposed a cycle that uses biomass and solar energy as renewable energies. Further, we will produce hydrogen and fresh water in this novel power plant. This plant can be used for many purposes, especially in sports facilities, and can pave the way for sustainable and clean sports facilities. Preheating gasification agent, by a PVT system, having a flexible energy generation because of the utilization of both solar and biomass energy with green hydrogen production, as well as double staged desalination unit make this system viable and unique. Furthermore, this system can provide clean water (which the shortage is alarming in some areas) and hydrogen to be used as a medical commodity (like hydrogen water or for recovery purposes of athletes) as well as an emergency storable fuel. Moreover, to simulate this system, we have analyzed it thermodynamically and exergoeconomically to assess its viability and applicability. Certainly, this will be useful and a great advancement for a better, abundant, and cleaner future.

2. System description and assumptions

2.1. System description

The six sub-cycles that comprise this proposed system are a water desalination RO unit, a PEM electrolyzer, a PVT system, and three power-generating layouts. The other two power-generating bottoming cycles run on the products of the gas Brayton cycle, which is regarded as the primary cycle. Preheated air from the PVT system gets injected into the gasifier in which biomass is converted into syngas and then burned in the combustion chamber (CC) to power the system. For optimal heat recovery, product gases also heat R365MFC by HE3 in the ORC and CO_2 by HE2 in the intercooling Bryton cycle. The numerous pumps in the double-staged RO unit get twenty percent of the power produced by the bottoming cycles. Furthermore, the RO unit uses the power produced by the Pelton turbine. The PVT system not only heats the air that is injected into the gasifier but also produces electricity that is exclusively used by the PEM electrolyzer to produce green hydrogen.

The first bottoming cycle is a supercritical CO_2 recompression with an intercooler which benefits from two heat recovery units. This power cycle is an efficient and practical layout that works in a suitable temperature range of exiting hot gases from HE1. The second bottoming cycle is regenerative ORC for the maximum heat recovery from exhaust gases. RO unit is comprised of two desalination filters and three pumps. These pumps increase the water pressure to the required amount for the filters to reach the desired level of desalination, the purpose of the booster pump (bp) is to repressurize the discharged saline to the required amount for the second stage of desalination. After the second stage water has a notable pressure which is utilized to run a Pelton turbine for maximum efficiency.

To save solar energy, we have allocated all the generated energy by the PVT unit to the PEM electrolyzer for green hydrogen generation. Furthermore, this solar-based unit preheats the gasification agent and increases the gasifier's exergy efficiency by around 2%. The general schematic of the suggested system is shown in Fig. 1.

2.2. Assumptions and key parameters

The thermodynamic simulation of the system takes certain presumptions into account. A few of the power system's crucial and significant parameters are included in Table 1. Tables 2 and 3 also represent key parameters of the PVT and PEM electrolyzer, respectively. The ambient temperature and pressure are taken to be 298 K and 101.3 kPa, respectively, and the system operates at a steady state. Furthermore, recuperators, condensers, and heat exchanger heat losses are disregarded.

3. System modeling

3.1. Thermodynamic modeling and analysis

This section aims to do a thermodynamic analysis by thermodynamically characterizing the system and its constituent parts. We model the current system under steady-state conditions, taking into account the pressure drop across the board and disregarding the potential and kinetic energy of individual streams. The equilibrium values for mass, energy, and exergy are expressed in Eq. (1) through (3) [45].

$$\sum \dot{m}_{in} - \sum \dot{m}_{out} = 0 \tag{1}$$

$$\dot{Q} - \dot{W} = \sum (\dot{m}h)_{in} - \sum (\dot{m}h)_{out} \tag{2}$$

$$\dot{E}x_{heat} - \dot{W} = \sum (\dot{m}ex)_{in} - \sum (\dot{m}ex)_{out} + \dot{E}x_{dest} \tag{3}$$

3.1.1. Gasifire

This thermochemical process of gasification involves the conversion of biomass into a gaseous mixture, known as syngas, through controlled partial oxidation. Syngas, primarily composed of carbon monoxide, hydrogen, and methane, serves as a valuable energy carrier with applications spanning electricity generation, heat production, and biofuel synthesis. The equilibrium model states that thermodynamic equilibrium should be reached by all gasifier reactions. The pyrolysis products are meant to burn and reach equilibrium in the reduction zone before they leave the gasifier. In the reduction zone, the following reactions occur [46]:

$$C + CO_2 \; 2CO \tag{4}$$

$$C + H_2O \; CO + H_2 \tag{5}$$

$$C + 2H_2 \; CH_4 \tag{6}$$

$$CO + H_2O \; CO_2 + H_2 \tag{7}$$

For methane formation, the equilibrium constant is [46]:

$$K_1 = \frac{P_{CH_4}}{(P_{H_2})^2} \tag{8}$$

while that for the shift reaction is [46]:

$$K_2 = \frac{P_{CO_2} P_{H_2}}{P_{CO} P_{H2O}} \tag{9}$$

According to Zainal et al. [46], the overall gasification reaction for the downdraft gasifiers can be written as:

$$C_XH_YO_Z + wh_2O + m(O_2 + 3.76N_2)\; n_1H_2 + n_2CO + n_3CO_2 + n_4H_2O + n_5CH_4 + n_6N_2 \tag{10}$$

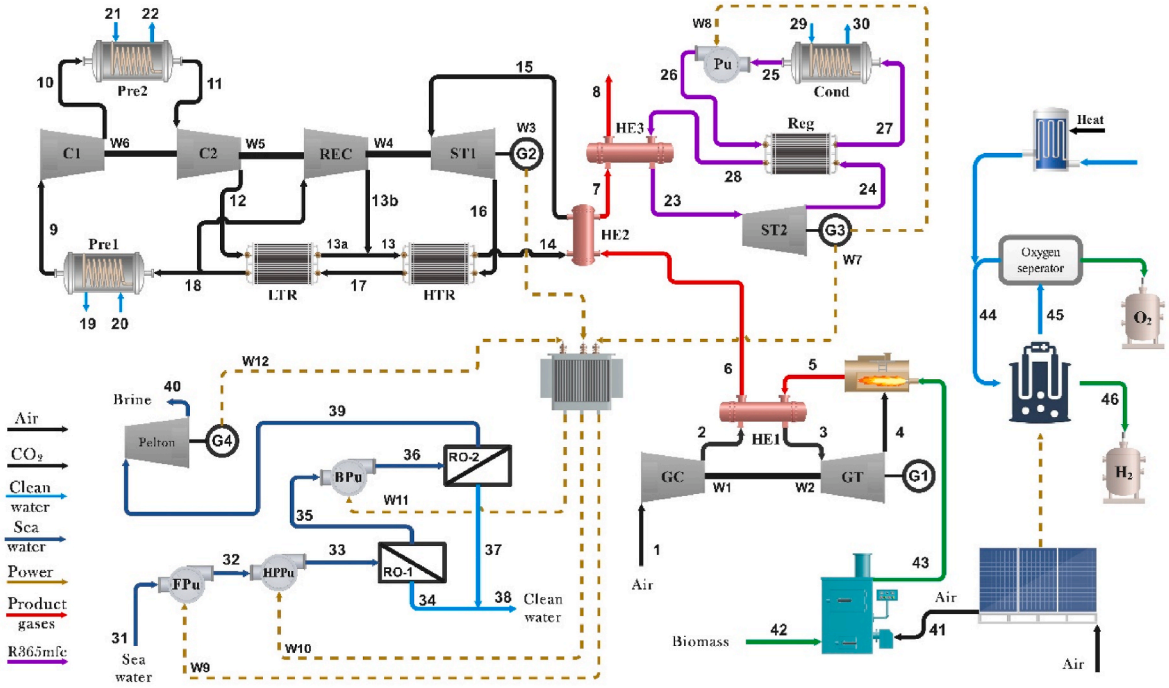

Fig. 1. Schematic of BCPVHR system.

Table 1
List of key parameters.

Parameter	Value
Gas turbine	
GTIT	1400 K
T_g	1073 K
T_6	800 K
AC r_p	10
ηis,AC	0.87
ηis,GT	0.89
SCO_2 cycle	
T_{15}	700 K
T_{19}, T_{21}, and T_{29}	298 K
P_{10}	11000 kPa
Maximum CO_2 pressure at Bryton cycle	2000 kPa
Minimum CO_2 pressure at Bryton cycle	7400 kPa
$\varepsilon_{HTR\ \&\ LTR}$	0.86
ηis, C1,C2,REC	0.89
ηis,T,CO2	0.9
ORC cycle	
T_{23}	500 K
Maximum R365fmc pressure	5000 kPa
Minimum R365fmc pressure	101.3 kPa
ηis,ST	0.9
ηis,Pu	0.8
ε_{Reg}	0.86
RO unit	
T_{water} in RO unit	298 K
ηis,FPu,HHPu,BPu	0.767
ηis,Pelton	0.79

Table 2
Input parameters for PVT system [42].

Parameter	Value	Parameter	Value or expression
β_c	0.83	α_b	0.90
τ_g	0.95	α_c	0.85
U_L (W/m^{2}K)	4.71	T_{sun} (K)	4500
h_{P2G}	0.1890	İ (kW/m^2)	1
h_{P1G}	0.9782	b	L (i.e., b = L)

Table 3
Input parameters for PEM electrolyzer [43,44].

Parameter	Value	Parameter	Value
T_{PEM} (K)	353	D (μm)	50
J_a^{ref} (A/m^2)	1.7×10^5	λ_a	14
J_c^{ref} (A/m^2)	4.6×10^3	λ_c	10
F (C/mol)	96486	$E_{act,a}$ (kJ/mol)	76
A_{PEM} (m^2)	0.0232	N	785

The molar amounts of water and oxygen per kmol of biomass are denoted by w and m, respectively, in Eq. (10). The primary constituents of biomass are carbon, hydrogen, and oxygen. According to Zainal et al. [46], wood has a higher heating value (HHV) of 449,568 kJ/kmol and composition of $CH_{1.44}O_{0.66}$, and wood is considered to be the selected biomass. MC denotes the moisture content per mole of wood, expressible as follows [46]:

$$MC = \frac{18w}{24 + 18w} \tag{11}$$

Therefore,

$$w = \frac{24MC}{18(1 - MC)} \tag{12}$$

Since MC is taken to be constant, w is considered to be fixed. We can determine the equilibrium constant values for methane generation and water-gas shift reactions by getting the values of the biofuel coefficient. The following equilibrium constants apply to methane generation Eq. (8) and the shift reaction Eq. (9), respectively [46]:

$$K_1 = \frac{n_5}{(n_1)^2} \tag{13a}$$

and

$$K_2 = \frac{n_3 n_1}{n_2 n_4} \tag{14a}$$

complete combustion reaction in the CC is as follows [46]:

$$n_1H_2 + n_2CO + n_3CO_2 + n_4H_2O + n_5CH_4 + n_6N_2 + n_{Air}\,(O_2 + 3.76\,N_2) \rightarrow n_7CO_2 + n_8H_2O + n_9O_2 + (n_6 + 3.76n_{air})N2 \quad (15a)$$

Extra information about the gasification process can be found in studies done by Zainal et al. [46] and Soltani et al. [47].

3.1.2. Reverse osmosis unit

The reverse osmosis module increases the pressure in the FPP and High-Pressure Pump (HPP) to convert saltwater into freshwater. Furthermore, a Pelton turbine provides a portion of the energy needed for the BPP. Using this energy, the pressure of the saline water that RO-1 releases is increased, allowing RO-2 to repeat the desalination process. The related equations of mass balance rate are [28]:

$$(\dot{m}y_s)_{33} = (\dot{m}y)_{34} + (\dot{m}y_s)_{35} \quad (16a)$$

$$(\dot{m}y_s)_{36} = (\dot{m}y)_{37} + (\dot{m}y_s)_{39} \quad (17a)$$

$$(\dot{m}y_s)_{38} = (\dot{m}y)_{38} + (\dot{m}y_s)_{34} \quad (18a)$$

Energy balance equations of the power generation system plus RO desalination unit are brought in Table 4.

3.2. Exergy equations

Exergy analysis is based on combining the equations controlling mass and energy balances with the concepts of the second law of thermodynamics. The formula for the exergy balance equation that is given emphasizes the importance of the boundary temperature (T) and the dead state temperature (T_o) in figuring out how quickly available energy dissipates inside a device. Furthermore, the rate of exergy linked with inflow or outflow from the device is represented by $\sum$Ex, highlighting the comprehensive nature of the analysis. $\dot{E}x_{di}$ represents the destruction of exergy in the i device [48].

$$\dot{E}x_{di} = \sum\left(1 - \frac{T_o}{T}\right)\dot{Q}_i - \dot{W}_i + \sum \dot{E}x_{in} - \sum \dot{E}x_{out} \quad (13b)$$

Dissipation of accessible energy in a system is closely related to entropy formation, where measurement of chemical and physical exergies at the component level becomes critical. As some components—like air—have constant compositions and so require little chemical energy, Reverse Osmosis cycles with their changing compositions require particular formulas (see Table 5). Equation (14) provides more information about how each component contributes to the total amount of energy that is wasted [48].

$$Y_k^* = \frac{\dot{E}x_{D,k}}{\dot{E}x_{D,total}} \quad (14b)$$

Exergy balance equations of the power generation system plus RO desalination unit are brought in Table 5.

3.3. Exergoeconomic analysis

The texts offered explore how exergetic and economic principles might be combined for system assessment, leading to the development of the exergoeconomic concept—which aims to minimize total cost as well as exergy loss. Using Eq. (15), which states that the cost rate of input exergy plus the component's investment cost rate equals the cost rate of output exergy, the evaluation's first section presents the cost equilibrium for the kth component. The approach calculates the cost rate of each stream ($\dot{C}$) by using a correlation constant called the average cost per unit of exergy (c). Table 6 provides comprehensive information about the auxiliary equations and cost balances required for each component of the system [48].

$$\dot{C}_{q,k} + \sum \dot{C}_{i,k} + \dot{Z}_k = \dot{C}_{w,k} + \sum \dot{C}_{e,k} \quad (15b)$$

$$\dot{C} = c \bullet \dot{E}x \quad (16b)$$

Here, Ż k is the summation of capital investments and maintenance

Table 4
Governing energy equations of the system.

Component	Energy balance equation
Gas Turbine	
Gas Compressor (GC)	$\dot{W}_{GC} = \dot{m}_1(h_2 - h_1)$
Gas Turbine (GT)	$\dot{W}_{GT} = \dot{m}_3(h_3 - h_4)$
Heat exchanger 1 (HE1)	$\dot{H}_2 + \dot{H}_5 = \dot{H}_3 + \dot{H}_6$
Combustion chamber (CC)	$(h_{air} + \bar{\lambda}\bar{h}_{fuel} - (1 + \bar{\lambda})h_{prod} = 0$
RO	
Feed pump (Fpu)	$\dot{W}_{Fpu} = \frac{\dot{V}_{31} \bullet \Delta P}{\mu_{Fpu}}$
High-pressure pump (HPpu)	$\dot{W}_{HPpu} = \frac{\dot{V}_{32} \bullet \Delta P}{\mu_{HPpu}}$
Boost pump (Bpu)	$\dot{W}_{Bpu} = \frac{\dot{V}_{35} \bullet \Delta P}{\mu_{Bpu}}$
Pelton Turbine (PT)	$\dot{W}_{PT} = \dot{m}_{39}(h_{39} - h_{40})$
R365MFC cycle	
Pump (Pu)	$\dot{W}_{Pu} = \dot{m}_{25}(h_{26} - h_{25})$
Condenser (Cond)	$\dot{Q}_{Cond} = \dot{m}_{27}(h_{27} - h_{25}), \dot{Q}_{Cond} = \dot{m}_{29}(h_{30} - h_{29})$
Regenerator (Reg)	$\dot{H}_{24} + \dot{H}_{26} = \dot{H}_{27} + \dot{H}_{28}$
S Turbine 2 (ST2)	$\dot{W}_{ST} = \dot{m}_{23}(h_{23} - h_{24})$
Heat Exchanger (HE3)	$\dot{H}_{28} + \dot{H}_7 = \dot{H}_{23} + \dot{H}_8$
SCO2 cycle	
HTR	$h_{16} - h_{17} = h_{14} - h_{13}$
LTR	$(1 - x)h_{13} - h_{12} = h_{17} - h_{18}$
Pre-cooler 1 (Pre1)	$\dot{Q}_{Pre1} = \dot{m}_{18}(h_9 - h_{18}), \dot{Q}_{pre1} = \dot{m}_{20}(h_{20} - h_{19})$
Pre-cooler 2 (Pre2)	$\dot{Q}_{Pre2} = \dot{m}_{10}(h_{11} - h_{10}), \dot{Q}_{pre2} = \dot{m}_{21}(h_{21} - h_{22})$
Compressor 1 (C1)	$\dot{W}_{C1} = \dot{m}_9(h_{10} - h_9)$
Compressor 2 (C2)	$\dot{W}_{C2} = \dot{m}_{11}(h_{12} - h_{11})$
REC	$\dot{W}_{REC} = \dot{m}_{18}(h_{13b} - h_{18})$
S Turbine 1 (ST1)	$\dot{W}_{ST1} = \dot{m}_{15}(h_{15} - h_{16})$

Table 5
Governing exergy equations of the system.

Component	Exergy balance equation
Gas Turbine	
Gas Compressor (GC)	$\dot{E}_1 + \dot{W}_{GC} = \dot{E}_2 + \dot{E}_{D,GC}$
Gas Turbine (GT)	$\dot{E}_3 + \dot{W}_{GT} = \dot{E}_4 + \dot{E}_{D,GT}$
Heat exchanger 1 (HE1)	$\dot{E}_2 + \dot{E}_5 = \dot{E}_3 + \dot{E}_6 + \dot{E}_{D,HE1}$
Combustion chamber (CC)	$\dot{E}_{43} + \dot{E}_4 = \dot{E}_5 + \dot{E}_{D,CC}$
RO	
Feed pump (Fpu)	$\dot{E}_{31} + \dot{W}_{Fpu} = \dot{E}_{32} + \dot{E}_{D,Fpu}$
High-pressure pump (HPpu)	$\dot{E}_{32} + \dot{W}_{HPpu} = \dot{E}_{33} + \dot{E}_{D,HPpu}$
Boost pump (Bpu)	$\dot{E}_{35} + \dot{W}_{Bpu} = \dot{E}_{36} + \dot{E}_{D,Bpu}$
Pelton Turbine (PT)	$\dot{E}_{39} = \dot{E}_{40} + \dot{W}_{PT} + \dot{E}_{D,PT}$
RO – 1	$\dot{E}_{33} = \dot{E}_{34} + \dot{E}_{35} + \dot{E}_{D,RO-1}$
RO – 2	$\dot{E}_{36} = \dot{E}_{37} + \dot{E}_{39} + \dot{E}_{D,RO-2}$
R365fmc cycle	
Pump (Pu)	$\dot{E}_{25} + \dot{W}_{Pu} = \dot{E}_{26} + \dot{E}_{D,Pu}$
Condunsor (Cond)	$\dot{E}_{27} + \dot{E}_{29} = \dot{E}_{25} + \dot{E}_{30} + \dot{E}_{D,Cond}$
Regenerator (Reg)	$\dot{E}_{24} + \dot{E}_{26} = \dot{E}_{27} + \dot{E}_{28} + \dot{E}_{D,HE3}$
S Turbine 2 (ST2)	$\dot{E}_{23} = \dot{E}_{24} + \dot{W}_{ST2} + \dot{E}_{D,ST2}$
Heat Exchanger (HE3)	$\dot{E}_{28} + \dot{E}_7 = \dot{E}_{23} + \dot{E}_8 + \dot{E}_{D,HE3}$
SCO_2 cycle	
HTR	$\dot{E}_{16} + \dot{E}_{13} = \dot{E}_{14} + \dot{E}_{17} + \dot{E}_{D,HTR}$
LTR	$\dot{E}_{13} + \dot{E}_{18} = \dot{E}_{17} + \dot{E}_{12} + \dot{E}_{D,LTR}$
Pre-cooler 1 (Pre1)	$\dot{E}_{18} + \dot{E}_{20} = \dot{E}_9 + \dot{E}_{19} + \dot{E}_{D,Pre1}$
Pre-cooler 2 (Pre2)	$\dot{E}_{10} + \dot{E}_{21} = \dot{E}_{11} + \dot{E}_{22} + \dot{E}_{D,Pre2}$
Compressor 1 (C1)	$\dot{E}_9 + \dot{W}_{C1} = \dot{E}_{10} + \dot{E}_{D,C1}$
Compressor 2 (C2)	$\dot{E}_{11} + \dot{W}_{C2} = \dot{E}_{12} + \dot{E}_{D,C2}$
REC	$\dot{E}_{18} + \dot{W}_{REC} = \dot{E}_{13b} + \dot{E}_{D,REC}$
S Turbine 1 (ST1)	$\dot{E}_{23} = \dot{E}_{24} + \dot{W}_{ST2} + \dot{E}_{D,ST2}$

Table 6
Exergoeconomic equations of the components in the system.

Component	Cost balance equation	Auxiliary equation
	Gas Turbine	
Gas Compressor (GC)	$\dot{C}_1 + \dot{Z}_{AC} = \dot{C}_2 + \dot{C}_{w,AC}$	$c_1 = 0$
Gas Turbine (GT)	$\dot{C}_3 + \dot{Z}_{GT} = \dot{C}_4 + \dot{C}_{w,GT}$	$c_3 = c_4$
Heat exchanger 1 (HE1)	$\dot{C}_2 + \dot{C}_5 + \dot{Z}_{HE1} = \dot{C}_3 + \dot{C}_6$	$c_5 = c_6$
Combustion chamber (CC)	$\dot{C}_{42} + \dot{C}_{fuel} + \dot{Z}_{CC} = \dot{C}_{43}$	$c_{fuel} = 2$
	RO	
Feed pump (Fpu)	$\dot{C}_{31} + \dot{C}_{w,FPu} + \dot{Z}_{FPu} = \dot{C}_{32}$	$c_{31} = 0$
High-pressure pump (HPpu)	$\dot{C}_{32} + \dot{C}_{w,HPPu} + \dot{Z}_{HPPu} = \dot{C}_{33}$	–
Boost pump (Bpu)	$\dot{C}_{35} + \dot{C}_{w,BPu} + \dot{Z}_{BPu} = \dot{C}_{36}$	–
Pelton Turbine (PT)	$\dot{C}_{39} = \dot{C}_{40} + \dot{C}_{w,PT} + \dot{Z}_{PT}$	–
RO – 1	$\dot{C}_{33} + \dot{Z}_{RO\_1} = \dot{C}_{34} + \dot{C}_{35}$	$c_{34} = c_{35}$
RO – 2	$\dot{C}_{36} + \dot{Z}_{RO\_2} = \dot{C}_{37} + \dot{C}_{39}$	$c_{37} = c_{39}$
	R365MFC cycle	
Pump (Pu)	$\dot{C}_{25} + \dot{C}_{w,Pu} + \dot{Z}_{Pu} = \dot{C}_{26}$	–
Condenser (Cond)	$\dot{C}_{27} + \dot{C}_{29} + \dot{Z}_{Cond} = \dot{C}_{25} + \dot{C}_{30}$	$c_{25} = c_{27}$, $c_{29} = 0$
Regenerator (Reg)	$\dot{C}_{24} + \dot{C}_{26} + \dot{Z}_{Reg} = \dot{C}_{27} + \dot{C}_{28}$	$c_{24} = c_{27}$
S Turbine 2 (ST2)	$\dot{C}_{23} + \dot{Z}_{ST2} = \dot{C}_{24} + \dot{C}_{w,ST2}$	$c_{23} = c_{24}$
Heat Exchanger 3 (HE3)	$\dot{C}_{28} + \dot{C}_7 + \dot{Z}_{HE3} = \dot{C}_{23} + \dot{C}_8$	$c_7 = c_8$
	SCO_2 cycle	
Heat exchanger 2 (HE2)	$\dot{C}_6 + \dot{C}_{14} + \dot{Z}_{HE2} = \dot{C}_7 + \dot{C}_{15}$	$c_7 = c_6$
HTR	$\dot{C}_{16} + \dot{C}_{13} + \dot{Z}_{HTR} = \dot{C}_{14} + \dot{C}_{17}$	$c_{16} = c_{17}$
LTR	$\dot{C}_{13} + \dot{C}_{18} + \dot{Z}_{LTR} = \dot{C}_{17} + \dot{C}_{12}$	$c_{18} = c_{17}$
Pre-cooler 1 (Pre1)	$\dot{C}_{18} + \dot{C}_{20} + \dot{Z}_{Pre1} = \dot{C}_9 + \dot{C}_{19}$	$c_9 = c_{18}$
Pre-cooler 2 (Pre2)	$\dot{C}_{10} + \dot{C}_{21} + \dot{Z}_{Pre2} = \dot{C}_{11} + \dot{C}_{22}$	$c_{10} = c_{11} = c_{21}$
Compressor 1 (C1)	$\dot{C}_9 + \dot{C}_{w,C1} + \dot{Z}_{C1} = \dot{C}_{10}$	–
Compressor 2 (C2)	$\dot{C}_{11} + \dot{C}_{w,C2} + \dot{Z}_{C2} = \dot{C}_{12}$	–
REC	$\dot{C}_{18} + \dot{C}_{w,REC} + \dot{Z}_{REC} = \dot{C}_{13b}$	–
S Turbine 1 (ST1)	$\dot{C}_{15} + \dot{Z}_{ST1} = \dot{C}_{16} + \dot{C}_{w,ST1}$	$c_{16} = c_5$

cost rates as follows [48]:

$$\dot{Z}_k = \dot{Z}_k^{CI} + \dot{Z}_k^{OM} = \varnothing_r \times \left(\frac{CRF}{N \times 3600}\right) Z_k \tag{17b}$$

Here, Z_k is the cost of purchased equipment related to the kth component, $\varnothing_r$ is the operation and maintenance factor, and CRF is the capital recovery factor. The expected life cycle (n) and interest rate (i) are used in the CRF computation in the following ways [48]:

$$CRF = \frac{i(1+i)^n}{(1+i)^n - 1} \tag{18b}$$

Emphasizing that component costs should be normalized by applying Eq. (19) to modify them from the reference year to the base year (2023):

$$Original\ cost = cost\ at\ refrence\ year \times \frac{cost\ index\ for\ the\ original\ year}{cost\ index\ for\ the\ refrence\ year} \tag{19}$$

Additionally, the exergoeconomic factor (f_k) is used to evaluate the components in detail. The exergoeconomic factor shows how important each component's non-exergy-related costs ($\dot{Z}_k$) and costs associated with exergy loss and destruction ($\dot{C}_{D,k} + \dot{C}_{L,k}$) are concerning each other.

$$f_k = \frac{\dot{Z}_k}{\dot{Z}_k + \dot{D}_{D,k} + \dot{C}_{L,k}} \tag{20}$$

$$r_k = \frac{c_{p,k} - c_{F,k}}{c_{F,k}} \tag{21}$$

Exergy balance equations of the power generation system plus RO desalination unit are brought in Table 6.

Also, the capital cost of each component (Z) is described as follows in Table 7 [49]:

3.4. PEM electrolyzer

The anode, electrolyte, and cathode are the three main components

Table 7
Capital cost equations of the components in the system.

Component	cost rate
Turbine 1	$Z_{T1} = \frac{479.34 \bullet \dot{m}_5}{0.92 - \eta T1} Ln\left(\frac{P_5}{P_6}\right)(1 + exp(0.036T_5 - 54.4))$
Compressor 1	$Z_{C1} = \frac{71.1 \bullet \dot{m}_1}{0.9 - \eta 283}\left(\frac{P_2}{P_1}\right) Ln\left(\frac{P_2}{P_1}\right)$
Compressor 2	$Z_{C2} = \frac{71.1 \bullet \dot{m}_{8b}}{0.9 - \eta C_2}\left(\frac{P_3}{P_8}\right) Ln\left(\frac{P_3}{P_8}\right)$
HTR, LTR, Pre-cooler	$Z_{HTR,LTR,pre} = 2681 A_{HTR,LTR,pre}^{0.59}$
Compressor	$Z_C = \left(\frac{75 \bullet \dot{m}_{air}}{0.9 - \eta_{is,C}}\right)\left(\frac{P_{out}}{P_{in}}\right) Ln\left(\frac{P_{out}}{P_{in}}\right)$
Combustion chamber	$Z_{CC} = 48.64 \bullet \dot{m}_{air(gas)} \bullet (1 + exp(0.018T_{out} - 26.4)) \bullet \left(\frac{1}{0.995 - \frac{P_{out}}{P_{in}}}\right)$
Gas Turbine	$Z_{GT} = \frac{1536 \bullet \dot{m}_{gas}}{0.92 - \eta_{is,GT}}\left(\frac{P_{out}}{P_{in}}\right)\left(1 + exp(0.036T_{in} - C_{34})\right)$
$HE_{1,2,3}$	$Z_{HE} = 4122 \bullet A_{HE}^{0.59}$ $U = 0.018\ kw/(m^2K)$
Gasifier	$Z_{gasifire} = 1600 \bullet \left(\dot{m}_{dry-biomass}\left[\frac{kg}{h}\right]\right)^{0.67}$
PEM	$Z_{PEM} = 1000\ \dot{W}_{PEM}$ ($)[a]
1PVT	$Z_{PVT} = 310 n_x n_y bL$[b] 2system ($n_x = 6$ and $n_y = 6$)

[a] Costs of the heat exchanger and O_2 separator are included.
[b] n_x and n_y are the number of cells in the width (b) and length (L) of the PVT.

that make up a PEM electrolyzer. Through the use of electricity, these units oxidize the injected water, producing protons and oxygen at the anode and electrons and hydrogen at the cathode. The created hydrogen is retained in the reservoir and oxygen is discharged [50]. Table 8 contains a collection of equations needed to represent and simulate these systems. Additional clarifications and broad details regarding PEM electrolyzers can be found in the research conducted by Ahmadi et al. [44].

3.5. Thermal photovoltaic system

Hydrogen production is powered by electricity from the PVT system. Additionally, the PVT system heats the air needed for the gasification of biomass. Modeling and simulating equations for the TPV system are shown in Table 9. The solar cell efficiency (η_c), packing factor (β_c), and transmissivity (τ_g) of the PVT glass are indicated in this table. The solar collector area (A) is measured in square meters. The overall heat transfer

Table 8
Modeling equations for PEM electrolyzers [44].

Total obtained energy	$\Delta H = \Delta G + T\Delta S$
Hydrogen mass flowrate	$\dot{N}_{H2,out} = \frac{J}{2F} = \dot{N}_{H2O,reacted}$
Input electricity	$E_{electric} = JV$
Overall losses	$V = V_0 + V_{act,a} + V_{act,cath} + V_{ohm}$
The reversible potential	$V_0 = 1.229 - 8.5 \times 10^{-4}(T_{PEM} - 298)$
Local ionic conductivity	$\sigma_{PEM}[\lambda(x)] = [0.5139\lambda(x) - 0.326]\exp\left[1268\left(\frac{1}{303} - \frac{1}{T}\right)\right]$
Membrane-electrode water content	$\lambda(x) = \frac{\lambda_a - \lambda_c}{D}x + \lambda_c$
Total Ohmic resistance	$R_{PEM} = \int_0^D \frac{dx}{\sigma_{PEM}[\lambda(x)]}$
Ohmic overpotential	$V_{ohm,PEM} = JR_{PEM}$
Activation overpotential	$V_{act,i} = \frac{RT}{F}\sinh^{-1}\left(\frac{J}{2J_{0,i}}\right), i = a, cath$
Exchange current density	$J_{0,i} = J_i^{ref}\exp\left(-\frac{E_{act,i}}{RT}\right), i = a, cath$

Table 9
Thermodynamic analysis expressions for PVT system [42].

Description	Parameters
Power production by PVT system	$W_{PV/T} = \eta_c \dot{I} \beta_c \tau_g$ A
Heat rate of glass-to-glass PVT system	$\dot{Q}_{solar} = \frac{\dot{m}_{air} Cp_{air}}{U_L} [(h_{P2G} Z\dot{I}) - U_L (T_{air,in} - T_0)] \times \left[1 - \exp\left(\frac{-bU_L L}{\dot{m}_{air} Cp_{air}}\right)\right]$
	$Z = \alpha_b \tau_g^2 (1-\beta_c) + h_{P1G} \tau_g \beta_c (\alpha_c - \eta_c)$
The outlet temperature of the air	$T_{air,output} = (T_0 + \frac{h_{P2G} Z\dot{I}}{U_L}) [1 - \frac{1 - \exp\left(\frac{-bU_L L}{\dot{m}_{air} Cp_{air}}\right)}{\frac{-bU_L L}{\dot{m}_{air} Cp_{air}}}]$
	$[T_{air,in} \frac{1 - \exp\left(\frac{-bU_L L}{\dot{m}_{air} Cp_{air}}\right)}{\frac{-bU_L L}{\dot{m}_{air} Cp_{air}}}]$
Energy efficiency of PVT system	$\eta_{PV/T} = \frac{\dot{Q} + \dot{W}_{PV/T}}{\dot{I} b U_L}$

coefficient (U_L) from the solar cell to the atmosphere through the top and back surfaces of the insulation is calculated. The absorptivities of a black surface and the solar cell are α_b and α_c, respectively. The penalty factors h_{P2G} and h_{P1G} are caused by the presence of the interface between the glass and the working fluid through the absorber plate and the presence of glass and ethylene-vinyl acetate for the glass-to-glass PVT system [42].

3.6. Overall performance and validation

The equations for energy and exergy efficiency of the BCPVHR are in Eq. (34) and Eq. (35). Meanwhile, the environmental index is shown in Eq. (36) [51].

$$\text{Energy efficiency} = \frac{\dot{W}_{net,cycle} + \dot{m}_{46} LHV_{H2}}{\dot{m}_{biomass} LHV_{biomass} + \dot{Q}_{sun}} \quad (34)$$

$$\text{Exergy efficiency} = \frac{\dot{W}_{net,cycle} + \dot{E}_{46}}{\dot{E}_{biomass} + \dot{E}_{sun}} \quad (35)$$

$$\zeta = (\dot{m}_{CO2} \ / \ \dot{W}_{net}) \times 3600 \ (\text{kWh}) \quad (36)$$

To simulate and adjust the individual parts as well as the system as a whole, we have employed Engineering Equation Slover (EES). As previously stated, the suggested downdraft gasifier operates in an equilibrium constant, similar to the research done by Zainal et al. [46]. In order to assess the validation process, we simulated a gasifier using wood as the biomass. Table 10 shows the outcomes of the validated model compared to Zainal's study [46].

The CO_2 intercooling cycle is validated and utilized by a study done by Lou et al. [52]. Fig. 2 demonstrates the minor differences between the current study and the mentioned reference. The maximum amount of error between the elicited result and the reference is 3% which occurs at multiple points.

The electrolyzer's J-V characteristics for the model under evaluation and the results of the experimental investigation conducted by Ioroi et al. [53] are shown in Fig. 3.

Table 10
Wood constituent breakdown comparison (in%).

Constituent	Present study model	Zainal equilibrium model [46]
Hydrogen	18.01	21.06
Carbon monoxide	18.77	19.61
Methane	0.68	0.64
Carbon dioxide	13.84	12.01
Nitrogen	48.7	46.68
Oxygen	0.00	0.00

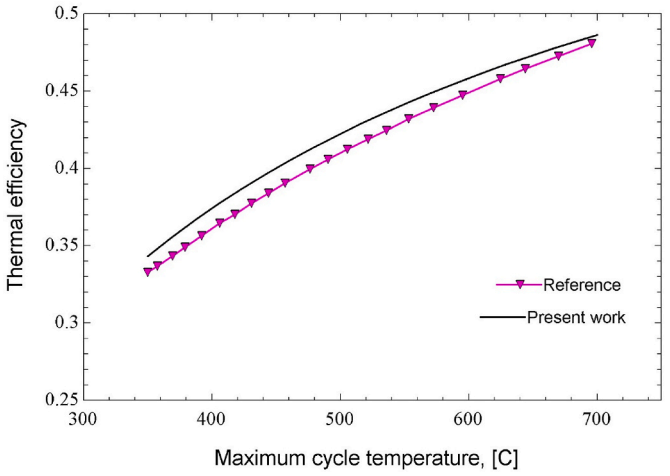

Fig. 2. Comparison of thermal efficiency of CO_2 intercooling cycle vs maximum cycle temperature in current study and the reference.

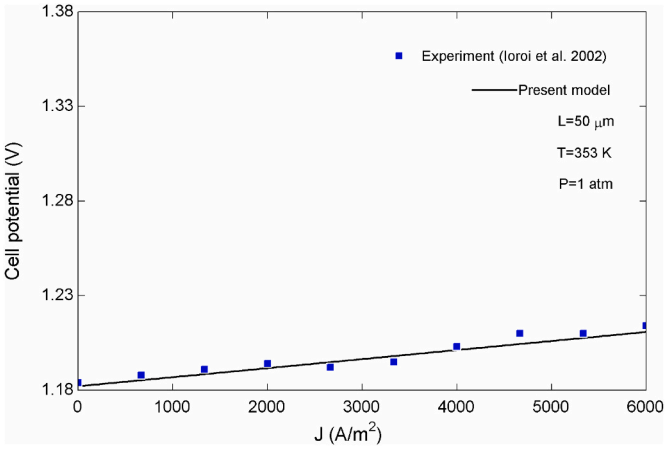

Fig. 3. Comparison between J-V characteristics of experimental study and current model.

The examined ORC has a regenerative layout which is thoroughly analyzed by Braimakis and Karellas [54]. Fig. 4 depicts the viability of the validated data using the mentioned reference.

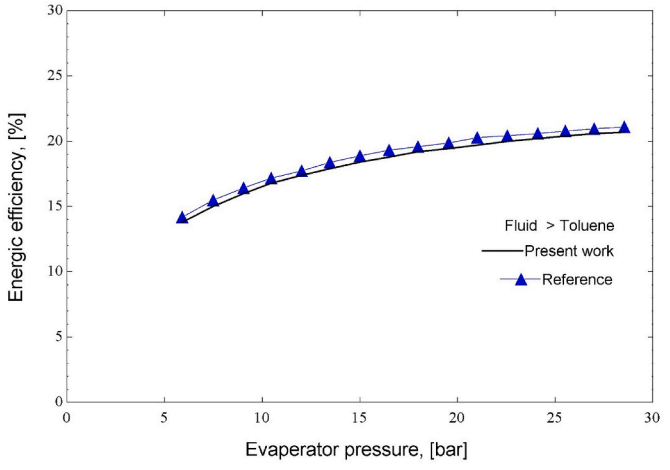

Fig. 4. Comparison between evaporator pressure vs energic efficiency of the reference study and current model.

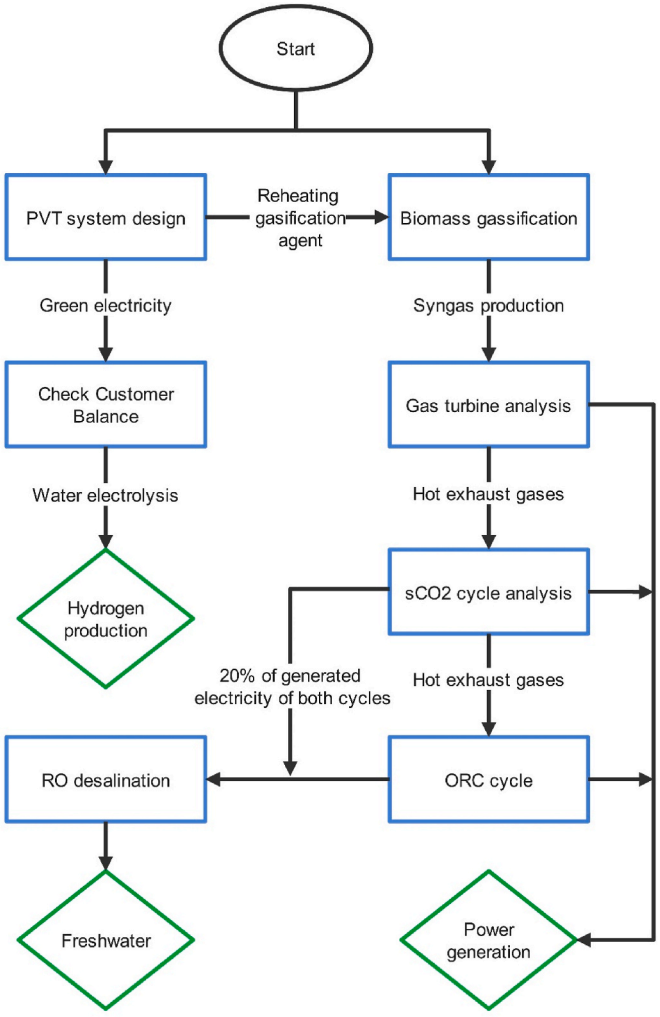

Fig. 5. Overall guide chart of the system.

Fig. 5 represents a guide chart for validation purposes and is shown below.

4. Results and discussion

4.1. Parametric study

The proposed system undergoes a parametric study to monitor the performance of the system based on some of its key parameters.

Variations of BCPVHR energy and exergy efficiencies, overall generated power, produced freshwater, environmental index, and levelized overall cost of products (LOCP) with compressor pressure ratio are shown in Fig. 6. As is evident in the figure, by increasing r_p there are optimum points for energy and exergy efficiencies. Optimum points are around $r_p = 11.5$. The reason for this pattern is due to the impact of r_p on the amount of power production in the cycle in which the power production rate is changed similar to the changes in energy and exergy efficiency. Hence, the energy and exergy efficiencies are influenced in this particular way.

Increasing the r_p with constant fuel consumption creates the optimum point for net generated power. The optimum point for generated power equals around $r_p = 11.5$. On the other hand, increasing the compressor pressure ratio first decreases the freshwater production until $r_p = 11.5$. Then fresh water production increases. Therefore, r_p after 11.5 has a favorable effect on water production. However, for net generated power that is not favorable. So, thorough decisions should be

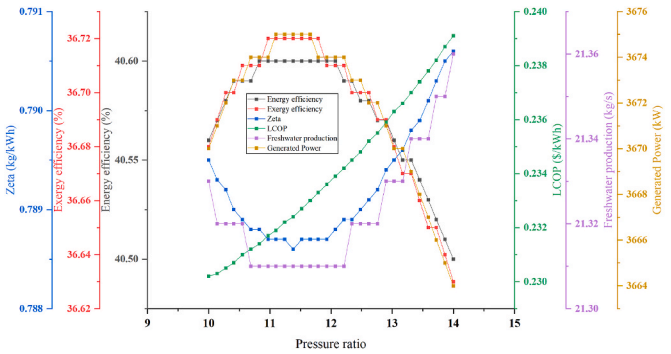

Fig. 6. Variations of BCPVHR energy and exergy efficiencies, overall generated power, produced freshwater, environmental index, and levelized overall cost of productions with r_p.

made based on the priority of production material. The reason for these changes is based on the equations which are mentioned in the analysis section.

Raising the compressor pressure ratio raises the plant LOCP and for the environmental index, there is an optimum point around 11.5, which is coincident with optimum points for energy and exergy efficiencies. All in all, the r_p increase is not useful as far as the economic perspective is concerned and regarding the environmental index till $r_p = 11.5$, that is efficient but after that value, it is detrimental to the environment.

Fig. 7 shows the variations of BCPVHR energy and exergy efficiencies, overall generated power, produced freshwater, environmental index, and LOCP with gas turbine inlet temperature. The trend for energy and exergy efficiency by GTIT is in an ascending way. With increasing the GTIT from 1000 K to 1400 K, energy efficiency increases from 29% to 40%. Meanwhile, by increasing the GTIT from 1000 K to 1400 K, the exergy efficiency of the plant increases in the range of 25% and 37%. The reason for this change is due to the higher power output of the gas turbine by higher GTIT.

As GTIT goes up, the net generated power gets higher and freshwater production decreases. Because the temperature in state 6 is constant, increasing GTIT lowers the mass flow rate of air therefore less combustion gas is available for the bottoming cycles. As mentioned earlier desalination unit utilizes a portion of the generated power by the bottoming cycles and it decreases freshwater production. Again, to adjust the required net generated power and fresh water the exact GTIT can be set.

As that is inferred from the plot, there are straightforward impacts on LOCP and environmental index as far as GTIT is concerned. Increasing the GTIT decreases the LOCP and environmental index. Increasing the gas temperature in the turbine is advantageous in both aspects and so

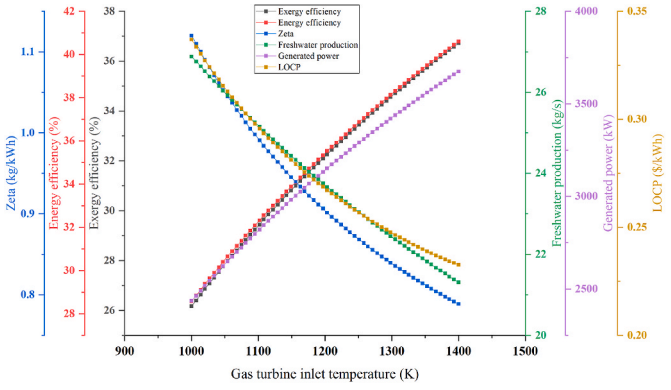

Fig. 7. Variations of BCPVHR energy and exergy efficiencies, overall generated power, produced freshwater, environmental index, and levelized overall cost of productions with gas turbine inlet temperature.

should be considered by engineers.

Fig. 8 depicts the variations of BCPVHR energy and exergy efficiencies, overall generated power, produced freshwater, environmental index, and LOCP with SCO_2 Brayton cycle turbine inlet temperature (STIT). As shown in this figure, increasing the STIT has a positive effect on energy and exergy efficiencies. By increasing the STIT, the turbine generates extra power and overshadows the extra consumed power by compressors in this cycle which results in rising the both efficiencies.

Net generated power and produced freshwater are crucial commodities of the presented system, therefore, with the rising trend of energy and exergy, it is expected that the amount of generated power and freshwater will increase as the STIT gets higher. According to the system's layout, the more power is generated, the more freshwater will be produced.

With increasing STIT both the total unit product cost and environmental index start to decrease which is a positive aspect for the system. This trend is predictable based on Fig. 7 as it shows that for a fixed amount of consumed fuel, the rising amount of net generated power results in economic and environmental efficiency.

Fig. 9 illustrates the changes gasification temperature causes to the system's efficiency, both from energy and exergy perspectives. It also shows how LOCP and environmental index react to this factor. As shown in this figure, low temperatures seem more beneficial in all aspects but these changes are not that significant. However, in most studies, this temperature is set to 800 °C (1073 K) because of its practicality [46].

Fig. 10 demonstrates the effect of the isentropic efficiency of air compressor on overall energy and exergy efficiencies, environmental index, and LOCP. It is evident that increasing the isentropic efficiency of this component (which is the top power consumer) drastically increases the overall efficiency of the system. However, it is clear that LOCP is minimum at around 0.87 which can be determined as an optimum point for isentropic efficiency. In many cases, the selected component has a predefined isentropic efficiency which is stated in Table 1 accordingly.

Fig. 11 illustrates the effect of GT isentropic efficiency on energy and exergy efficiencies, environmental index, and LOCP. As GT is the most productive component in terms of power generation, changes in isentropic efficiency have a dramatic effect on the system's efficiency. With raising the value of isentropic efficiency both efficiencies increase and the environmental index decreases which are positive effects. However, in terms of LOCP, there is an optimal point around 0.87 which minimizes the price of products.

4.2. Case study

Utilizing the preferred and optimal parameters of the present system, we can monitor the thermodynamic characteristics of each state in the system as well as the exergy efficiency of each component. Tables 11a and 11b show the thermodynamic properties of both the power generation system and the RO desalination system, respectively. The exergy efficiency of each component in the system is depicted in Fig. 12a and b.

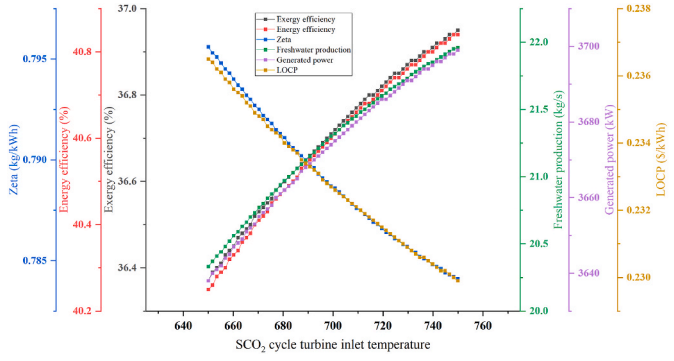

Fig. 8. Variations of BCPVHR energy and exergy efficiencies, overall generated power, produced freshwater, environmental index, and levelized overall cost of productions with SCO_2 cycle turbine inlet temperature.

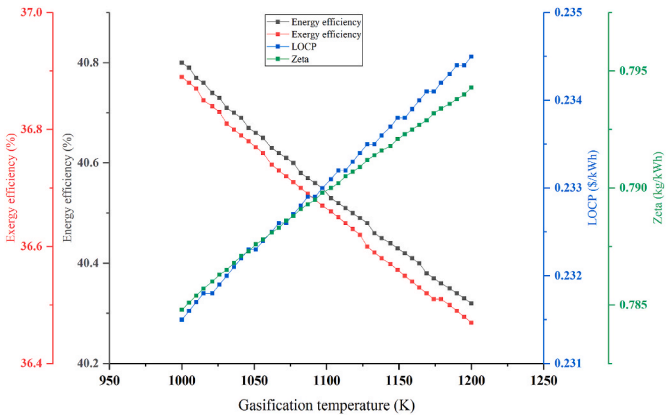

Fig. 9. Variation of energy and exergy efficiencies, environmental index, and LOCP with gasification temperature.

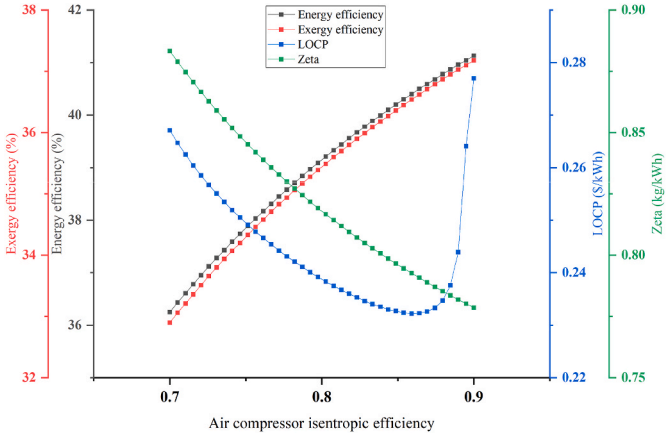

Fig. 10. Variation of energy and exergy efficiencies, environmental index, and LOCP with air compressor isentropic efficiency.

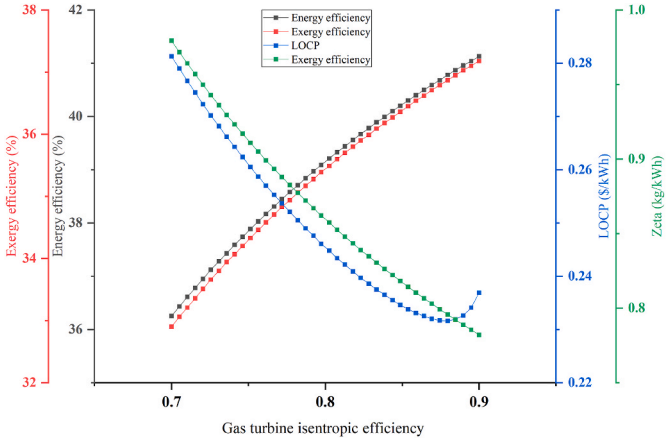

Fig. 11. Variation of energy and exergy efficiency with gas turbine and compressor isentropic efficiency.

5. Conclusion

The new power plant for being used partially or completely in sports

Table 11a
Thermodynamic characteristics of given states (power generation layout).

State	T (K)	P (kPa)	Molar enthalpy (kJ/kmol)	Molar entropy (kJ/kmol K)	Ė (kW)	Mass flow rate (kg/s)
1	298	101.3	−4.366	194.3	0	9.219
2	633.6	1165	10012	196.4	2998	9.219
3	1400	1165	35330	222.4	8615	9.219
4	833.5	101.3	16300	225.4	2253	9.219
5	1456	101.3	317.4	245.2	8330	10
6	800	101.3	−22803	224.2	2429	10
7	605.9	101.3	−29106	215.1	1163	10
8	408.4	101.3	−35241	202.9	292.8	10
9	305.2	7630	−8600	−60.54	2421	11.25
10	310.9	9156	−8473	−60.49	2451	11.25
11	305.2	9156	−9839	−64.92	2439	11.25
12	308.7	10987	−9715	−64.88	2467	11.25
13	337.3	10987	−3829	−46.64	3228	14.06
14	565.9	10987	10163	−13.92	4584	14.06
15	700	10987	17065	−2.982	5748	14.06
16	659.9	7630	15220	−2.67	5128	14.06
17	382.5	7630	1228	−30.25	3283	14.06
18	319.1	7630	−3224	−43.1	3084	14.06
19	298.2	101.3	1890	6.615	0	32.88
20	308.2	101.3	2643	9.099	23.23	32.88
21	298.2	101.3	1890	6.615	0	8.352
22	308.2	101.3	2643	9.099	5.9	8.352
23	500	5000	89185	299	807	8.079
24	395.6	101.3	79083	302.8	193.1	8.079
25	313.3	101.3	37725	175.7	2.957	8.079
26	315.5	5000	38462	176.2	35.59	8.079
27	326.7	101.3	67700	271.3	35.59	8.079
28	368.4	5000	49845	209.5	114.9	8.079
29	298.2	101.3	1890	6.615	0	39.13
30	308.2	101.3	2643	9.099	27.64	39.13

Table 11b
Thermodynamic characteristics of given states (RO desalination unit).

State	T (C)	P (kPa)	Enthalpy (kJ/kg)	Entropy (kJ/kg K)	Ė (kW)	Mass flow rate (kg/s)
31	15	101	59.74	0	20.62	26.72
32	15	320	59.94	0.1819	26.32	26.72
33	15	6230	65.34	5.091	180.1	26.72
34	15	110	63.06	1.917	50.33	14.7
35	15	5940	62.8	3.174	83.31	12.02
36	15	7050	63.79	3.581	96.26	12.02
37	15	110	63.05	1.078	22.37	6.613
38	15	110	59.75	2.995	72.65	21.31
39	15	6850	65.91	2.503	51.94	5.018
40	15	150	59.79	0.9308	19.31	5.018

facilities is proposed. This plant uses a biomass gasification unit to provide the required fuel in the plant. Meanwhile, solar energy is harnessed in this plant via PVT unit and hydrogen is produced as a valuable energy carrier by PEM. Furthermore, fresh water is produced by reverse osmosis water purification unit. It is imperative to modify and improve conventional power plants for a more sustainable layout. The products can be used in sports facilities. The main varying parameters are compressor pressure ratio and gas turbine inlet temperature. The proposed BCPVHR plant is analyzed based on energy, exergy, and exergoeconomic analyses, and environmental index. The main findings are:

- ✓ Increasing the r_p leads to the optimum point for energy efficiency, exergy efficiency, and, environmental index at around $r_p = 11.5$. Power generation is at maximum while freshwater production is at its lowest amount for this value.
- ✓ Increasing the GTIT, increases the energy and exergy efficiencies and decreases the both total unit product cost and the environmental index. Also, it increases the net generated power and decreases the freshwater production.

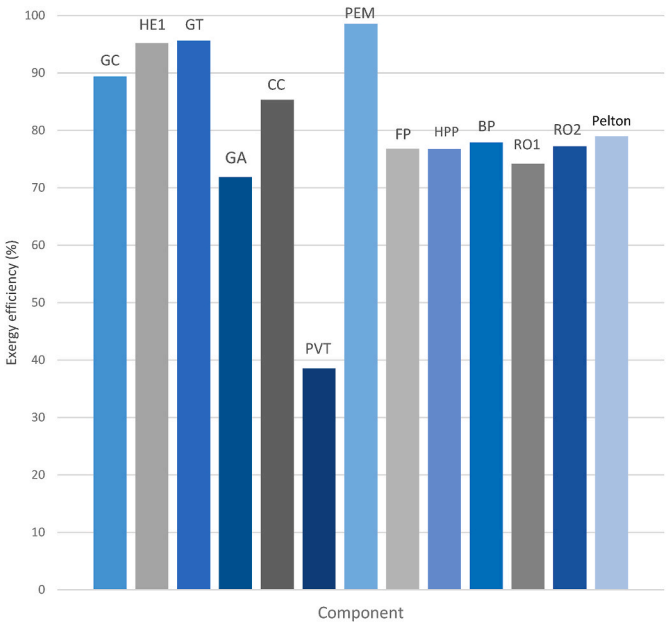

Fig. 12a. Exergy efficiency of components (main cycle, PVT, PEM, and RO unit).

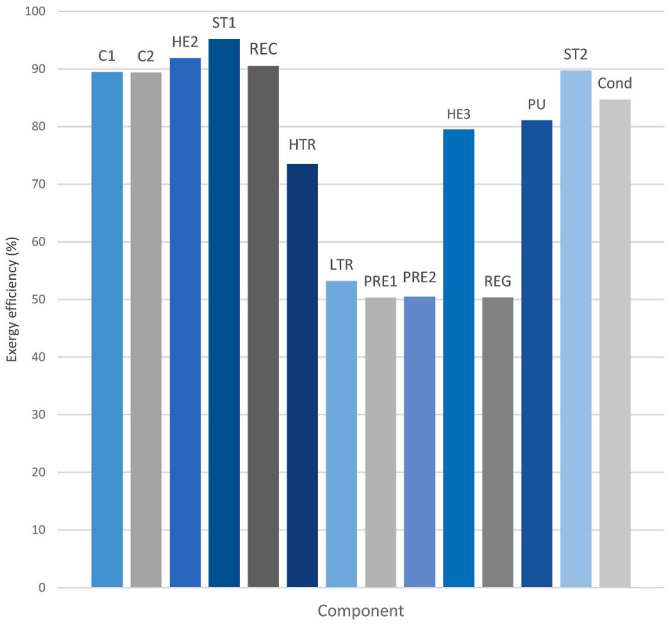

Fig. 12b. Exergy efficiency of components (bottomin cycles).

Preheating gasification agent by PVT unit increases the energy efficiency of the system by around 2%. It is obvious that increasing the scale of the PVT unit improves the preheating process but with economical drawbacks. It is notable that with 0.5 kmol/s biomass injection and other constant parameters mentioned in the tables, we were able to achieve energy and exergy efficiencies, hydrogen and freshwater production, power generation, total product cost, and, the environmental index of 40.6, 36.7, 7.54 kmol/h, 21.3 kg/s, 3675 kW, 64.6 $/GJ, and 0.78 kg/kWh, respectively.

Based on the findings reported in this work the BCPVHR is a valuable power plant and its features are measured and these findings can be used by engineers for the construction of sports facilities.

Declaration of competing interest

The authors declare that they have no known competing financial interests or personal relationships that could have appeared to influence the work reported in this paper.

References

[1] Wang Z, et al. Thermal evolution of chemical structure and mechanism of oil sands bitumen. Energy 2022;244:123190.
[2] Renewables I. Analysis and forecast to 2026. Paris, France: International Energy Agency; 2021.
[3] Hu G, et al. Design, analysis and optimization of a hybrid fluid flow magnetorheological damper based on multiphysics coupling model. Mech Syst Signal Process 2023;205:110877.
[4] Liu L, Tang Y, Liu D. Investigation of future low-carbon and zero-carbon fuels for marine engines from the view of thermal efficiency. Energy Rep 2022;8:6150–60.
[5] Yang C, et al. Degradation mechanism and modeling study on reversible solid oxide cell in dual-mode—a review. Int J Hydrogen Energy 2022;47(89):37895–928.
[6] Li H-M, et al. Combustion characteristics and concentration measurement of ADN-based liquid propellant with electrical ignition method in a combustion chamber. Fuel 2023;344:128142.
[7] Tian H, et al. Bi-objective optimization and environmental assessment of SOFC-based cogeneration system: performance evaluation with various organic fluids. Process Saf Environ Protect 2023;178:311–30.
[8] Ding J, Somani A. A long-term investment planning model for mixed energy infrastructure integrated with renewable energy. In: 2010 IEEE green technologies conference. IEEE; 2010.
[9] Wang X, et al. High performance and stable perovskite solar cells using vanadic oxide as a dopant for spiro-OMeTAD. J Mater Chem A 2019;7(21):13256–64.
[10] Lyu SO. Unveiling willingness to pay for green stadiums: insights from a choice experiment. J Clean Prod 2024;434:139985.
[11] Morán-Gámez G, et al. Measuring green practices in sport: development and validation of a scale. Sustainability 2024;16(2):494.
[12] Sfintes R. Football stadium: an energy-efficient building and a source of renewable energy for the community. Energy Efficient Building Design; 2020. p. 171–84.
[13] Rachmat B, et al. Concept of computational fluid dynamics and its application in sport science: bibliometric analysis of modelling thermal comfort in sport Hall. CFD Lett 2024;16(1):1–21.
[14] Mallen C, Chard C, Sime I. Web communications of environmental sustainability initiatives at sport facilities hosting major league soccer. J. Mgmt. & Sustainability 2013;3:115.
[15] Widdop P, Anagnostopoulos C, Parnell D. The business of the FIFA world cup. Routledge, Taylor & Francis Group; 2022.
[16] Chard C, Mallen C. Renewable energy initiatives at Canadian sport stadiums: a content analysis of web-site communications. Sustainability 2013;5(12):5119–34.
[17] Wanless L, Seifried C, Kellison T. Renewable energy source diffusion in professional sport facilities. J Sport Manag 2023;1(aop):1–13.
[18] Trendafilova S, et al. Environmental sustainability in sport: current state and future trends. Global Journal on Advances Pure and Applied Sciences 2014;3(1):9–14.
[19] Artuso P, Santiangeli A. Energy solutions for sports facilities. Int J Hydrogen Energy 2008;33(12):3182–7.
[20] Abouemara K, et al. The review of power generation from integrated biomass gasification and solid oxide fuel cells: current status and future directions. Fuel 2024;360:130511.
[21] Chen X, et al. Performance analysis of a novel biomass gasification system coupled to a coal-fired power plant based on heat and water recovery. Energy Convers Manag 2024;299:117822.
[22] Perea-Moreno M-A, Samerón-Manzano E, Perea-Moreno A-J. Biomass as renewable energy: worldwide research trends. Sustainability 2019;11(3):863.
[23] Fu C, et al. Determining the optimal biomass-gasification-based fuel cell trigeneration system in exergy-based cost and carbon footprint method considering energy level. Energy Convers Manag 2024;299:117802.
[24] Amjith L, Bavanish B. A review on biomass and wind as renewable energy for sustainable environment. Chemosphere 2022;293:133579.
[25] Naqvi SAA, et al. Environmental sustainability and biomass energy consumption through the lens of pollution Haven hypothesis and renewable energy-environmental kuznets curve. Renew Energy 2023;212:621–31.
[26] Tahir F, Saeed MA, Ali U. Biomass energy perspective in Pakistan based on chemical looping gasification for hydrogen production and power generation. Int J Hydrogen Energy 2023;48(48):18211–32.
[27] Baroutaji A., et al. Additive manufacturing for Proton Exchange Membrane (PEM) hydrogen technologies: merits, challenges, and prospects. Int J Hydrogen Energy 2023; 52 (part A): 561-584.
[28] Wang Y, et al. The multi-scenario projection of cost reduction in hydrogen production by proton exchange membrane (PEM) water electrolysis in the near future (2020–2060) of China. Fuel 2023;354:129409.
[29] Folgado FJ, González I, Calderón AJ. PEM Electrolyzer Digital Replica based on internal resistance determination applied to hydrogen energy storage. J Energy Storage 2024;75:109694.
[30] Wang K, et al. Operando analysis of in-plane heterogeneity for the PEM electrolyzer cell: mappings of temperature and current density. J Clean Prod 2024: 140586.
[31] Marshall A, et al. Hydrogen production by advanced proton exchange membrane (PEM) water electrolysers—reduced energy consumption by improved electrocatalysis. Energy 2007;32(4):431–6.
[32] Al-Waeli AH, et al. A review of photovoltaic thermal systems: achievements and applications. Int J Energy Res 2021;45(2):1269–308.
[33] Al-Waeli AH, et al. Photovoltaic/Thermal (PV/T) systems: status and future prospects. Renew Sustain Energy Rev 2017;77:109–30.
[34] Melaibari AA, et al. New design for PVT system with elliptic cooling duct involving nanofluid in existence of MHD and utilizing TEG. Case Stud Therm Eng 2024;53: 103815.
[35] Gao Y, et al. A comprehensive review of the current status, developments, and outlooks of heat pipe photovoltaic and photovoltaic/thermal systems. Renewable Energy; 2023.
[36] Joshi SS, Dhoble AS. Photovoltaic-Thermal systems (PVT): technology review and future trends. Renew Sustain Energy Rev 2018;92:848–82.
[37] Namin AS, Rostamzadeh H, Nourani P. Thermodynamic and thermoeconomic analysis of three cascade power plants coupled with RO desalination unit, driven by a salinity-gradient solar pond. Therm Sci Eng Prog 2020;18:100562.
[38] Xiao T, et al. Integration of desalination and energy conversion in a thermo-osmotic system using low-grade heat: performance analysis and techno-economic evaluation. Appl Therm Eng 2023;223:120039.
[39] Greenlee LF, et al. Reverse osmosis desalination: water sources, technology, and today's challenges. Water Res 2009;43(9):2317–48.
[40] Chen K, et al. Hydrophilic-hydrophobic bilayer interlayer for high performance thin-film composite reverse osmosis membranes. J Membr Sci 2024;689:122177.
[41] Beni AN, et al. Membrane properties overview in integrated forward osmosis/osmotically assisted reverse osmosis systems. Desalination 2024;569:117008.
[42] Moharramian A, et al. Modified exergy and modified exergoeconomic analyses of a solar based biomass co-fired cycle with hydrogen production. Energy 2019;167: 715–29.
[43] Nami H, Akrami E, Ranjbar F. Hydrogen production using the waste heat of Benchmark pressurized Molten carbonate fuel cell system via combination of organic Rankine cycle and proton exchange membrane (PEM) electrolysis. Appl Therm Eng 2017;114:631–8.
[44] Ahmadi P, Dincer I, Rosen MA. Energy and exergy analyses of hydrogen production via solar-boosted ocean thermal energy conversion and PEM electrolysis. Int J Hydrogen Energy 2013;38(4):1795–805.
[45] Dincer I, Rosen MA. Exergy and energy analyses. Exergy; 2013. p. 21–30.
[46] Zainal Z, et al. Prediction of performance of a downdraft gasifier using equilibrium modeling for different biomass materials. Energy Convers Manag 2001;42(12): 1499–515.
[47] Soltani S, et al. Thermodynamic analyses of an externally fired gas turbine combined cycle integrated with a biomass gasification plant. Energy Convers Manag 2013;70:107–15.
[48] Bejan A, Tsatsaronis G, Moran MJ. Thermal design and optimization. John Wiley & Sons; 1995.
[49] Moharramian A, et al. Conventional and enhanced thermodynamic and exergoeconomic analyses of a photovoltaic combined cycle with biomass post firing and hydrogen production. Appl Therm Eng 2019;160:113996.
[50] Falcão D, Pinto A. A review on PEM electrolyzer modelling: guidelines for beginners. J Clean Prod 2020;261:121184.
[51] Gharamaleki FP, et al. A novel sustainable biomass-fueled cogeneration cycle integrated with carbon dioxide capture utilizing LNG regasification and green hydrogen production via PEM electrolysis: thermodynamic assessment. J Clean Prod 2023;421:138529.
[52] Luo D, Huang D. Thermodynamic and exergoeconomic investigation of various SCO2 Brayton cycles for next generation nuclear reactors. Energy Convers Manag 2020;209:112649.
[53] Ioroi T, et al. Thin film electrocatalyst layer for unitized regenerative polymer electrolyte fuel cells. J Power Sources 2002;112(2):583–7.
[54] Braimakis K, Karellas S. Energetic optimization of regenerative organic rankine cycle (ORC) configurations. Energy Convers Manag 2018;159:353–70.